Effects of Functionalization, Catenation, and Variation of the Metal Oxide and Organic Linking Units on the Low-Pressure Hydrogen Adsorption Properties of Metal−Organic Frameworks

Jesse L. C. Rowsell and Omar M. Yaghi*

*Contribution from the Department of Chemistry, University of Michigan,
930 North University Avenue, Ann Arbor, Michigan 48109*

Received September 28, 2005; E-mail: oyaghi@umich.edu

Abstract: The dihydrogen adsorption isotherms of eight metal−organic frameworks (MOFs), measured at 77 K up to a pressure of 1 atm, have been examined for correlations with their structural features. All materials display approximately Type I isotherms with no hysteresis, and saturation was not reached for any of the materials under these conditions. Among the six isoreticular MOFs (IRMOFs) studied, the catenated materials exhibit the largest capacities on a molar basis, up to 9.8 H_2 per formula unit. The addition of functional groups ($-Br$, $-NH_2$, $-C_2H_4-$) to the phenylene links of IRMOF-1 (MOF-5), or their replacement with thieno[3,2-*b*]thiophene moieties in IRMOF-20, altered the adsorption behavior by a minor amount despite large variations in the pore volumes of the resulting materials. In contrast, replacement of the metal oxide units with those containing coordinatively unsaturated metal sites resulted in greater H_2 uptake. The enhanced affinities of these materials, MOF-74 and HKUST-1, were further demonstrated by calculation of the isosteric heats of adsorption, which were larger across much of the range of coverage examined, compared to those of representative IRMOFs. The results suggest that under low-loading conditions, the H_2 adsorption behavior of MOFs can be improved by imparting larger charge gradients on the metal oxide units and adjusting the link metrics to constrict the pore dimensions; however, a large pore volume is still a prerequisite feature.

Introduction

Hydrogen storage has been a consistently topical and controversial focus of materials research over the past few decades. The recent increased activity in the field is due to the growing recognition of the negative consequences of fossil fuel-based energy dependency. The storage of this lightweight fuel is just one of the challenges impeding the realization of its potential benefits, but its solution will be crucial for the transportation sector, currently the largest consumer of oil and consequently a major source of airborne pollutants. Due to its low critical temperature, the storage of dihydrogen is primarily an issue of volume; for mobile fueling a sufficient amount of the gas must be compressed under very high pressure (several hundreds of atmospheres) or maintained as a liquid at very low temperature (20 K). In both cases, the issue of safe handling and refueling is paramount. Further optimization of these physical methods is not believed to be sufficient for widespread implementation of hydrogen as a transportation fuel source, and therefore, chemical storage methods are being explored.[1]

Hydrogen storage materials fall into two categories: those that dissociate the molecules and chemically bind them as hydrides and those that physisorb the molecules on their surfaces. Clearly, the most important attributes of the second class are high surface area and strong binding potential; thus, microporous adsorbents such as activated carbons and zeolites have been examined.[2] More recently, a new class of microporous adsorbents has received attention for their comparable, if not greater, apparent surface areas and pore volumes. Metal−organic frameworks (MOFs) are crystalline, infinite networks assembled by the bonding of metal ions with polyfunctional organic molecules. Their attributes include high porosity, spatial and chemical tailoring, and synthetic scalability. Application of these functional materials, particularly toward gas storage and separation, is now a focus of considerable research.[3]

Our recent discussion of current progress in the development of MOFs as hydrogen storage materials presented strategies for improving their properties and emphasized the need to broaden our current knowledge of the potential of these materials.[4] There are several thousand MOF structures already reported, but only

(1) (a) *Basic Research Needs for the Hydrogen Economy*; United States Department of Energy, Report of the Basic Energy Sciences Workshop on Hydrogen Production, Storage, and Use, May 13−15, 2003. http://www.sc.doe.gov/ bes/hydrogen.pdf. (b) Tzimas, E.; Filiou, C.; Peteves, S. D.; Veyret, J.-B. *Hydrogen Storage: State-of-the-Art and Future Perspective*: European Commission DG JRC Institute for Energy, Petten, 2003. http://www.jrc.nl/publ/2003_publ.html.

(2) (a) Bénard, P.; Chahine, R. *Langmuir* **2001**, *17*, 1950. (b) Nijkamp, M. G.; Raaymakers, J. E. M. J.; van Dillen, A. J.; de Jong, K. P. *Appl. Phys. A* **2001**, *72*, 619. (c) Becher, M.; et al. *C. R. Phys.* **2003**, *4*, 1055.

(3) (a) Rowsell, J. L. C.; Yaghi, O. M. *Microporous Mesoporous Mater.* **2004**, *73*, 3. (b) Kitagawa, S.; Kitaura, R.; Noro, S.-I. *Angew. Chem., Int. Ed.* **2004**, *43*, 2334. (c) Janiak, C. *Dalton Trans.* **2003**, 2781.

(4) Rowsell, J. L. C.; Yaghi, O. M. *Angew. Chem., Int. Ed.* **2005**, *44*, 4670.

a fraction of these have been studied for this purpose. A logical examination of the structure−property trends of the most promising candidates is required. Through this undertaking, the structural characteristics that most strongly influence the H_2 adsorptive capacity of MOFs may be elucidated and provide direction for future studies. We[5,6] and others[7,8,9] have begun such systematic studies on small subsets of MOFs and related materials, with the early recognition that both the capacities and heats of adsorption could be substantially varied.

We now present data where chemical functionality, catenation, and metal oxide secondary building unit structure have been varied to gauge their relative importance. Improved syntheses are presented for several known materials and one new MOF, the porosities of which have been experimentally demonstrated to be among the largest ever reported. In comparing their dihydrogen adsorption isotherms, measured at 77 K and up to 1 atm, correlations with their crystallographically resolved structural features have been determined. These were further examined by isosteric analysis of H_2 adsorption data collected at other temperatures. The results suggest that under low loading conditions, the H_2 adsorption behavior of MOFs can be improved by imparting larger charge gradients on the metal oxide units and adjusting the link metrics to constrict the pore dimensions; however, a large pore volume is still a prerequisite feature.

Experimental Section

Sample Preparation. Detailed syntheses and characterization results are listed below for each material in this study. All samples were prepared by solvothermal methods from a solution or slurry of the starting materials, which included the nitrate salt of the metal ion and the conjugate acid of the linking organic carboxylate. In most cases, large single or twinned crystals of the desired phase were formed, providing initial optical confirmation of product purity. The as-synthesized materials were then rinsed with *N,N*-dimethylformamide (DMF, Fisher) to remove unreacted reagents, and immersed in the appropriate activation solvent to exchange the occluded solvent. After activation, the materials were evacuated in situ within the adsorption apparatus prior to adsorption measurements. Characterization of the porous materials was performed by powder X-ray diffraction (Bruker AXS D8 Advance diffractometer, Bragg−Brentano geometry, Cu Kα radiation), FT-IR spectroscopy (Perkin-Elmer Spectrum BX, KBr pellet, 4000−400 cm⁻¹), and elemental analysis (Department of Chemistry, University of Michigan).

IRMOF-2, $Zn_4O(C_8H_3BrO_4)_3$. 2-Bromobenzene-1,4-dicarboxylic acid (0.38 g, 1.6 mmol, Aldrich) and zinc nitrate tetrahydrate (1.5 g, 5.7 mmol, EM Science) were dissolved in 100 mL of *N,N*-diethylformamide (BASF) with stirring in a 1-L wide mouth glass jar. The jar was tightly capped and placed in a 100 °C oven for 40 h to yield cubic crystals. After decanting the hot mother liquor and rinsing with DMF, the product was immersed in chloroform (Fisher) for 3 d, during which the activation solvent was decanted and freshly replenished three times. The solvent was removed under vacuum at room temperature, yielding the porous material. Elemental analysis (EA) (% calc/found): C 28.6/28.7, H 0.90/0.85, N 0/<0.1, Zn 26.0/23.7. FT-IR: 3370 (br), 1942 (w), 1579 (s), 1534 (sh), 1484 (m), 1386 (s), 1280 (sh), 1253 (m),

1146 (w), 1037 (m), 907 (w), 888 (w), 829 (m), 802 (w), 767 (m), 734 (w), 661 (w), 541 (m).

IRMOF-3, $Zn_4O(C_8H_5NO_4)_3$. 2-Aminobenzene-1,4-dicarboxylic acid (0.75 g, 4.1 mmol, Aldrich) and zinc nitrate tetrahydrate (3.0 g, 11 mmol, EM Science) were dissolved in 100 mL of *N,N*-diethylformamide (BASF) with stirring in a 1-L wide mouth glass jar. The jar was tightly capped and placed in a 100 °C oven for 18 h to yield cubic crystals. After decanting the hot mother liquor and rinsing with DMF, the product was immersed in chloroform (Fisher) for 3 d, during which the activation solvent was decanted and freshly replenished three times. The solvent was removed under vacuum at room temperature, yielding the porous material. Elemental analysis (EA) (% calc/found): C 35.4/35.5, H 1.86/2.00, N 5.16/5.39, Zn 32.1/28.8. FT-IR: 3366 (br), 1619 (sh), 1568 (s), 1499 (m), 1419 (s), 1383 (s), 1258 (m), 1154 (w), 1124 (w), 1064 (w), 947 (w), 898 (w), 834 (m), 796 (m), 768 (m), 696 (w), 582 (w), 515 (w).

IRMOF-6, $Zn_4O(C_{10}H_6O_4)_3$. 1,2-Dihydrocyclobutabenzene-3,6-dicarboxylic acid (1.0 g, 5.2 mmol, prepared as described in the literature[10]) and zinc nitrate tetrahydrate (3.0 g, 11 mmol, EM Science) were dissolved in 100 mL of *N,N*-diethylformamide (BASF) with stirring in a 1 L wide mouth glass jar. The jar was tightly capped and placed in a 100 °C oven for 18 h to yield cubic crystals. After decanting the hot mother liquor and rinsing with DMF, the product was immersed in chloroform (Fisher) for 3 d, during which the activation solvent was decanted and freshly replenished three times. The solvent was removed under vacuum at room temperature, yielding the porous material. Elemental analysis (EA) (% calc/found): C 42.5/42.7, H 2.14/2.03, N 0/<0.1, Zn 30.8/27.1. FT-IR: 3392 (br), 2972 (w), 2929 (w), 1930 (w), 1579 (s), 1486 (m), 1392 (s), 1332 (sh), 1227 (w), 1199 (m), 1137 (m), 1026 (w), 934 (w), 863 (w), 811 (m), 775 (m), 741 (w), 669 (w), 630 (w), 593 (w), 538 (w), 480 (w).

IRMOF-9, $Zn_4O(C_{14}H_8O_4)_3$. 4,4′-Biphenyldicarboxylic acid (0.3 g, 1.2 mmol, Aldrich) and zinc nitrate tetrahydrate (1.8 g, 6.9 mmol, EM Science) were stirred for 15 min in 100 mL of *N,N*-dimethylformamide (Fisher) in a 1-L wide mouth glass jar. The jar was tightly capped and placed in a 100 °C oven for 18 h to yield rectangular prismatic crystals. After decanting the hot mother liquor and rinsing with DMF, the product was immersed in chloroform (Fisher) for 3 d, during which the activation solvent was decanted and freshly replenished three times. The solvent was removed under vacuum at room temperature, yielding the porous material. Elemental analysis (EA) (% calc/found): C 50.5/50.2, H 2.42/2.18, N 0/<0.1, Zn 26.2/23.4. FT-IR: 3200 (br), 1934 (w), 1607 (sh), 1581 (s), 1530 (s), 1394 (s), 1270 (sh), 1178 (m), 1143 (w), 1104 (w), 1019 (w), 1004 (m), 874 (w), 852 (m), 796 (w), 767 (s), 700 (m), 681 (m), 583 (w), 534 (w), 446 (w).

IRMOF-13, $Zn_4O(C_{18}H_8O_4)_3$. Pyrene-2,7-dicarboxylic acid (0.1 g, 0.34 mmol, prepared by hydrolysis of the dimethyl ester[11]) and zinc nitrate tetrahydrate (0.6 g, 2.3 mmol, EM Science) were stirred for 15 min in 100 mL of *N,N*-dimethylformamide (Fisher) in a 1-L wide mouth glass jar. The jar was tightly capped and placed in a 70 °C oven for 40 h to yield trigonal block crystals. After decanting the hot mother liquor and rinsing with DMF, the product was immersed in chloroform (Fisher) for 3 d, during which the activation solvent was decanted and freshly replenished three times. The solvent was removed under vacuum at room temperature, yielding the porous material. Elemental analysis (EA) (% calc/found): C 56.8/53.7, H 2.12/1.95, N 0/<0.1, Zn 22.9/21.1. FT-IR: 3400 (br), 3037 (w), 2925 (w), 1927 (w), 1800 (w), 1601 (s), 1558 (s), 1459 (s), 1384 (s), 1375 (sh), 1313 (sh), 1256 (m), 1126 (w), 1104 (w), 1000 (w), 904 (m), 818 (m), 768 (w), 744 (m), 703 (m), 599 (w), 500 (w), 446 (w).

IRMOF-20, $Zn_4O(C_8H_2O_4S_2)_3$. Thieno[3,2-*b*]thiophene-2,5-dicarboxylic acid (0.75 g, 3.3 mmol, prepared as described in the literature[12])

(5) Rosi, N. L.; Eckert, J.; Eddaoudi, M.; Vodak, D. T.; Kim, J.; O'Keeffe, M.; Yaghi, O. M. *Science* **2003**, *300*, 1127.
(6) Rowsell, J. L. C.; Millward, A. R.; Park, K. S.; Yaghi, O. M. *J. Am. Chem. Soc.* **2004**, *126*, 5666.
(7) Chun, H.; Dybstev, D. N.; Kim, H.; Kim, K. *Chem. Eur. J.* **2005**, *11*, 3521.
(8) Zhao, X.; Xiao, B.; Fletcher, A. J.; Thomas, K. M.; Bradshaw, D.; Rosseinsky, M. J. *Science* **2004**, *306*, 1012.
(9) Kaye, S. S.; Long, J. R. *J. Am. Chem. Soc.* **2005**, *127*, 6506.

(10) Walker, K. A.; Markoski, L. J.; Moore, J. S. *Synthesis* **1992**, 1265.
(11) Connor, D. M.; Allen, S. D.; Collard, D. M.; Liotta, C. L.; Schiraldi, D. A. *J. Org. Chem.* **1999**, *64*, 6888.
(12) (a) Bugge, A. *Acta Chem. Scand.* **1968**, *22*, 63. (b) Fuller, L. S.; Iddon, B.; Smith, K. A. *J. Chem. Soc., Perkin Trans. 1* **1997**, 3465.

and zinc nitrate tetrahydrate (3.0 g, 11 mmol, EM Science) were dissolved in 100 mL of *N,N*-diethylformamide (BASF) with stirring in a 1-L wide mouth glass jar. The jar was tightly capped and placed in a 100 °C oven for 18 h to yield cubic crystals. After decanting the hot mother liquor and rinsing with DMF, the product was immersed in chloroform (Fisher) for 3 d, during which the activation solvent was decanted and freshly replenished three times. The solvent was removed under vacuum at room temperature, yielding the porous material. Elemental analysis (EA) (% calc/found): C 30.1/29.8, H 0.63/0.90, N 0/<0.1, S 20.1/18.3, Zn 27.4/23.4. FT-IR: 3378 (br), 3088 (w), 1575 (s), 1481 (s), 1382 (s), 1324 (s), 1173 (m), 1099 (m), 900 (w), 857 (w), 764 (m), 688 (m), 534 (w), 499 (w), 439 (w).

HKUST-1, $Cu_2(C_9H_3O_6)_{4/3}$. Benzene-1,3,5-tricarboxylic acid (5.0 g, 24 mmol, Aldrich) and copper(II) nitrate hemipentahydrate (10.0 g, 43 mmol, Aldrich) were stirred for 15 min in 250 mL of solvent consisting of equal parts *N,N*-dimethylformamide (Fisher), ethanol (Fisher) and deionized water in a 1-L wide mouth glass jar. The jar was tightly capped and placed in an 85 °C oven for 20 h to yield small octahedral crystals. After decanting the hot mother liquor and rinsing with DMF, the product was immersed in dichloromethane (Fisher) for 3 d, during which the activation solvent was decanted and freshly replenished three times. The solvent was removed under vacuum at 170 °C, yielding the porous material. Elemental analysis (EA) (% calc/ found): C 35.7/35.7, H 1.00/1.49, N 0/<0.1, Cu 31.5/29.5. FT-IR: 3440 (br), 1706 (w), 1645 (s), 1587 (m), 1449 (m), 1374 (s), 1112 (w), 1060 (w), 1004 (w), 938 (w), 761 (m), 730 (m), 587 (w), 490 (w).

MOF-74, $Zn_2(C_8H_2O_6)$. 2,5-Dihydroxybenzene-1,4-dicarboxylic acid (2.5 g, 13 mmol, Aldrich) and zinc nitrate tetrahydrate (10.0 g, 38 mmol, EM Science) were dissolved in 500 mL of *N,N*-dimethyl-formamide (Fisher) with stirring in a 1-L wide mouth glass jar. After dissolution of the reagents, 25 mL of deionized water was added. The jar was tightly capped and placed in an 100 °C oven for 20 h to yield trigonal block crystals. After decanting the hot mother liquor and rinsing with DMF, the product was immersed in methanol (Fisher) for 6 d, during which the activation solvent was decanted and freshly replen-ished three times. The solvent was removed under vacuum at 270 °C, yielding the porous material. Elemental analysis (EA) (% calc/found): C 29.6/28.5, H 0.62/0.61, N 0/0.18, Zn 40.3/36.5. FT-IR: 3400 (br), 2457 (w), 1616 (sh), 1553 (s), 1457 (m), 1429 (sh), 1406 (s), 1365 (m), 1240 (m), 1193 (m), 1121 (w), 882 (m), 813 (m), 581 (w), 503 (w).

Single-Crystal X-ray Diffraction. The structure of IRMOF-20 was determined by single crystal X-ray diffraction and found to be isoreticular with other IRMOFs previously reported. A colorless block crystal (0.34 mm × 0.30 mm × 0.23 mm) was sealed in a capillary and analyzed at 258 K: cubic space group $Fm\bar{3}m$ with $a = 29.184(3)$ Å, $V = 24\ 856(4)$ Å^3, $Z = 8$. Data were collected using graphite-monochromated Mo Kα radiation on a Bruker SMART APEX diffractometer system. A total of 17084 reflections were collected in the range $1.97° < \theta < 24.72°$ of which 1121 were independent and 860 were observed ($I > 2\sigma[I]$). The Bruker SHELXTL program was used to solve the structure using direct methods techniques. All stages of weighted full-matrix least-squares refinement were conducted using F_o^2 data with the Bruker SHELXTL software package and converged to give $R_1 = 10.6\%$ and $wR_2 = 32.5\%$ ($I > 2\sigma[I]$). These values are typical for compounds of this type that contain large volume fractions of disordered solvent. Application of the SQUEEZE routine in the PLATON software package[13] reduced these values to $R_1 = 3.41\%$ and $wR_2 = 9.34\%$ ($I > 2\sigma[I]$), $S = 1.001$. The quality of the refinement was further limited by the two-fold site disorder exhibited by the linking moiety, which was not resolvable in the other space groups examined. This type of disorder is also common among MOF structures composed of links with rotable bonds, and also among several molecular structures containing the thieno[3,2-*b*]thiophene moiety.

Adsorption Measurements. Dinitrogen and dihydrogen isotherms were measured gravimetrically at 77 K using a previously described method.[14] A Cahn C-1000 microgravimetric balance was used to measure the change in mass of samples suspended within a glass enclosure under a chosen atmosphere. Samples were outgassed in situ according to the conditions listed above until constant mass was attained; these varied from 0.2 to 2.0 g. Prior to admittance of the analyte gas, the entire chamber and manifold were evacuated overnight while the walls were heated several times using a heat gun. The system was purged at room temperature three times with the analyte gas before cooling to 77 K, and gases were passed through a molecular sieve trap before being exposed to the sample. When hydrogen gas was used, the trap was additionally immersed in liquid nitrogen to remove any condensable impurities. Pressures were measured with two MKS Baratron transducers 622A with the range covering 0−10 and 0−1000 Torr (accuracy 0.25%). The adsorbate was added incrementally, and data points were recorded when no further change in mass was observed. An empirical buoyancy correction was applied to all data points based on the change in mass of standard aluminum foil weights within the analyte gas at 77 K. Volumetric adsorption measurements were performed at 77, 87, and 195 K using an Autosorb-1 from Quantachrome Instruments on properly outgassed (see individual procedures above) samples 100−200 mg in mass.

Structural Calculations. The surface area and pore volume of each material were calculated using the Connolly method[15] and "Available Free Volume" calculation within Cerius^2 (Accelrys) was applied to the crystal structure data using a probe radius of 1.82 Å, which is appropriate for N_2. Pore volumes were also calculated using the "calc solv probe [x]" command within PLATON,[13] with $x = 1.8$ Å. To reduce inaccuracies generated by framework atom site disorder, ordered models of each structure were generated in lower symmetry space groups where necessary. For noncatenated IRMOFs, space group $Pa\bar{3}$ was used with the same cell parameter. The asymmetric unit which describes an ordered variant of the $Fm\bar{3}m$ structure includes two Zn atoms, one O atom, and all of the atoms of one molecular link.

Results and Discussion

Isoreticular Metal−Organic Frameworks (IRMOFs). The materials studied here display many of the important attributes that have generated interest in MOFs during the past decade. One of these is preparative scalability. Conditions for the growth of large, high-quality single crystals in good yield were first optimized in small scale using 20-mL scintillation vials as reaction vessels. It was found that with slight adjustments of concentration and fractional volume filling the reaction condi-tions could be extended to 1-L vessels. Variables in the reaction conditions include time, temperature, reagent concentrations, solvent type, and fractional volume filling of the vessel. The synthetic conditions of IRMOFs are similar, requiring excess Zn^{2+} and concentrations of link that approach saturation at room temperature.[16] The similarity in preparations was also observed here; however, we found that alteration of temperature and solvent aided in the preparation of some IRMOFs composed of links with limited solubility. It was also noted that the fractional volume filling of the vessel had an appreciable effect on the yields and crystal quality of the products, presumably due to a difference in the density of heterogeneous nucleation sites on the walls and bottom of the glass vessel.

The common preparative conditions for IRMOFs lead to another of their attributes, the ability to alter their framework

(13) Spek, A. L. *J. Appl. Crystallogr.* **2003**, *36*, 7.

(14) Eddaoudi, M.; Li, H.; Yaghi, O. M. *J. Am. Chem. Soc.* **2000**, *122*, 1391.
(15) Connolly, M. *J. Am. Chem. Soc.* **1985**, *107*, 1118.
(16) Eddaoudi, M.; Kim, J.; Rosi, N.; Vodak, D.; Wachter, J.; O'Keeffe, M.; Yaghi, O. M. *Science* **2002**, *295*, 469.
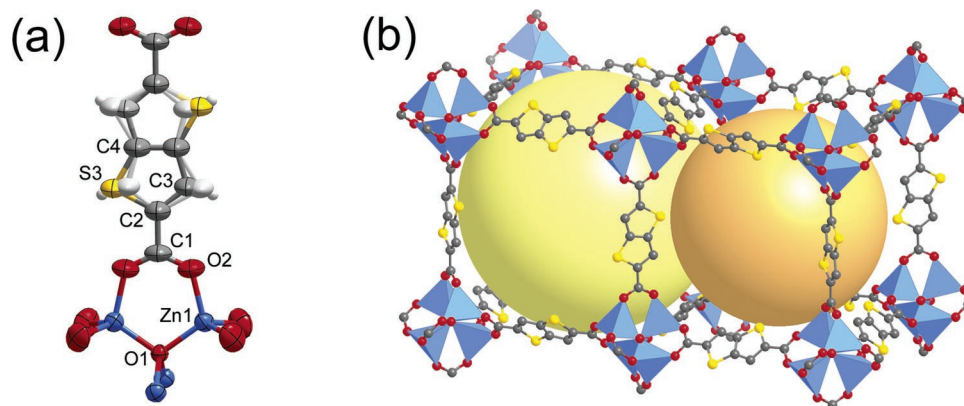
Figure 1. (a) Thermal ellipsoid plot of a fragment of the IRMOF-20 structure with the atoms of the asymmetric unit labeled. Ellipsoids are plotted at 50% probability with hydrogen atoms shown as small spheres. One orientation of the disordered link is shown in color, the alternate atomic positions of the other are shown in light gray. Atom colors: C dark gray, H white, O red, S orange, Zn blue. (b) The framework connectivity of IRMOF-20 with the zinc coordination sphere shown as blue tetrahedra. Two approximately spherical pores, shown as large yellow and orange spheres, are defined, which intersect at the apertures.

metrics and functionality by adroit choice of organic link. All MOFs are in principle reticulated through the connection of metal ions by polycoordinating ligands; however, in only a few instances has a structurally predictive capability been exerted to produce porous frameworks. IRMOFs are composed of linear linking moieties connecting octahedral $Zn_4O(O_2C-)_6$ secondary building units (SBUs), resulting in frameworks based on the same primitive cubic topology (or more accurately the augmented version thereof, analogous to the B net in CaB_6).[16] By determining the synthetic conditions that favor the formation of this secondary building unit over the many others that are possible, a material with a desired functionality can be produced by imparting that functionality in the organic starting material.

One structural feature that may influence the amount of hydrogen adsorbed by an IRMOF is the electronic character of the linking organic units. These contain phenylene or polyaromatic cores with available positions for chemical functionalization, as demonstrated by IRMOF-1, -2, -3, and -6, prepared from benzene-1,4-dicarboxylic acid and its bromo-, amino-, and dihydrocyclobuta- derivatives, respectively. The structures of these compounds have been reported previously.[16] In this study, we have also demonstrated that heteroatoms can be incorporated in the aromatic backbone of the organic links, by using thieno[3,2-*b*]thiophene-2,5-dicarboxylic acid as the precursor to IRMOF-20. The structure of this compound was confirmed to be isoreticular with others of this series by structural refinement of single-crystal X-ray diffraction (see Supporting Information). The framework has pores that are 17.3 and 14.0 Å in diameter, as illustrated in Figure 1. Similar attempts were made to produce an IRMOF linked by pyridine-2,5-dicarboxylate; however, only salts of molecular chelate complexes were obtained.

A common activation procedure was also found to facilitate the evacuation of the IRMOF frameworks, the crucial step in preparing the porous materials for adsorptive evaluation. The occluded solvent in the as-synthesized samples is first exchanged with chloroform by immersion. This step replaces the strongly interacting guest formamide solvent molecules (possibly as well as reactant molecules and/or solvent decomposition products) with more weakly interacting chloroform molecules that are easily removed under vacuum at room temperature, minimizing pore blockage and framework collapse.[16] The resulting materials

were determined to be microporous by their Type I adsorption isotherms for N_2 at 77 K. The importance of this activation step is apparent; for instance, highly porous IRMOF-1 samples have not been produced by heating alone[17] (although an alternate synthetic procedure was used, producing materials with PXRD intensities that deviate significantly from those calculated from the single-crystal structure). Highly porous IRMOF-1 has been prepared independently with a similar activation procedure, and its large apparent surface area was confirmed by argon adsorption.[9]

From the dinitrogen adsorption data, the apparent monolayer surface area and pore volume of each material has been estimated. For comparison with other reported materials, both the Langmuir and BET models have been used to calculate the apparent surface area, although it is recognized that for these microporous materials the mechanism of adsorption is pore filling rather than mono- or multilayer coverage.[18] The linearized BET equation was fit to data within the range $0.02 < P/P^0 < 0.3$, and the apparent surface areas were calculated using a molecular cross-sectional area of 16.2 Å² for both models. The results are presented in Table 1. The BET areas are generally 25−30% less than the Langmuir areas, as often recorded in the literature. The pore volume of each material was determined by extrapolating the Dubinin−Radushkevich equation across the linear region of the low-pressure data points with the assumption that the density of the adsorbate in the pore was the same as the liquid state. From the gravimetric values (in cm³/g), the volumetric values were obtained using the evacuated crystal densities. In all cases, the values are substantial; greater than for zeolites and most activated carbons.

The measured porosity indicators of each material can be compared with values calculated from their crystallographic structure data. Surface areas were calculated using the method of Connolly[15] with a probe radius equivalent to the kinetic radius of N_2. These values show similar trends as the experimental results and are typically 15−30% greater than the Langmuir areas. It is tempting to ascribe these discrepancies to incomplete sample evacuation or partial collapse of the networks; however,

(17) (a) Huang, L.; Wang, H.; Chen, J.; Wang, Z.; Sun, J.; Zhao, D.; Yan, Y. *Micropor. Mesopor. Mater.* **2003**, *58*, 105. (b) Panella, B.; Hirscher, M. *Adv. Mater.* **2005**, *17*, 538.
(18) Rouquerol, F.; Rouquerol, J.; Sing, K. *Adsorption by Powders & Porous Solids*; Academic Press: London, UK, 1999.

Table 1. Summary of Porosity Measurements, Calculations and Hydrogen Adsorption Data for Materials in This Study[a]

material	A_{Lang} (m²/g)	A_{BET} (m²/g)	A_{Conn} (m²/g)	V_p (cm³/g)	V_p [b] (cm³/cm³)	V_{C2} (cm³/cm³)	V_{PLAT} (cm³/cm³)	N_{H2} (mg/g)	H₂ per f.u.[c]	f_{H2} (%)
IRMOF-2	2544	1722	2780	0.88	0.69	0.773	0.719	12.1	6.0	19.4
IRMOF-3	3062	2446	3613	1.07	0.68	0.776	0.740	14.2	5.7	18.7
IRMOF-6	3263	2476	3987	1.14	0.74	0.757	0.710	14.8	6.2	18.3
IRMOF-9	2613	1904	3558	0.90	0.59	0.741	0.679	11.7	5.8	18.4
IRMOF-13	2100	1551	3072	0.73	0.55	0.696	0.625	17.3	9.8	33.5
IRMOF-20	4346	3409	3275	1.53	0.78	0.838	0.803	13.5	6.4	12.5
HKUST-1	2175	1507	3270	0.75	0.66	0.718	0.626	25.4	5.1	47.8
MOF-74	1132	783	1880	0.39	0.48	0.640	0.558	17.7	2.9	64.1

[a] Acronyms: A_{Lang}, A_{BET}, A_{Conn} are the Langmuir, BET, and calculated Connolly apparent surface areas; V_p is the measured pore volume; V_{C2}, V_{PLAT} are the calculated pore volumes using Cerius² and PLATON; N_{H2} is the amount of H₂ adsorbed at 1 atm, 77 K; $f_{H2} = N_{H2}/(1000 \times \rho_{H2} \times V_p)$ is the fraction of the pore volume filled by liquid H₂ ($\rho_{H2} = 0.0708$ g/cm³) at 1 atm and 77 K. [b] Converted from the gravimetric values using the crystal densities of the evacuated materials. [c] Formula units (f.u.) defined as Zn_4OL_3 for IRMOFs, $Cu_2L_{4/3}$ for HKUST-1, and Zn_2L for MOF-74, where **L** is the corresponding organic link.

since it is clear that pore filling and not monolayer coverage is the correct description of the adsorption mechanism in these materials, we present their values for comparison purposes only. It is more likely that the first layer of adsorbate is simply not as efficiently packed as the convolutions of the Connolly surface describe, and this is not sufficiently compensated by the additional apparent surface area that is due to adsorbate in a second or higher layer. The agreement between the measured and calculated (Cerius²) pore volumes is better, typically within 15%. These values can also be compared with those calculated by PLATON (see Table 1), which are 5−10% less than those of Cerius². For very open frameworks such as these, it was observed that the calculated pore volume was weakly dependent on the probe radius, which leads to a 2−3% decrease in volume upon increasing from 1.2 to 2.0 Å. Similarly, the alteration of grid spacing in the Cerius² calculations did not have an appreciable effect on the pore volume for values below 1 Å (PLATON uses a grid spacing of ∼0.2 Å). However, for structures with narrow channels or apertures, these factors may be more influential; therefore, it is necessary to perform calculations using a probe radius corresponding to the adsorptive.

As expected from their large porosities, the materials adsorb considerable amounts of dihydrogen. Isotherms measured at 77 K are shown in Figure 2 for the noncatenated IRMOFs-2, -3, -6, and -20 along with the previously reported data for IRMOF-1.[6] The rapid mass equilibration (∼10 min per step) and absence of hysteresis confirmed that dihydrogen is reversibly physisorbed by the materials. In addition to adsorbing comparable amounts at 1 atm (12−15 mg/g), the isotherm curvature is very similar for these materials, indicating that the chemical differences in the organic links play only a minor role in the adsorption under these conditions. This is emphasized by normalizing the data for the differences in masses of the links, as shown in Figure 2 and listed in Table 1.

These observations corroborate some recent computational studies of the interaction of dihydrogen with the organic and inorganic fragments of the IRMOF structure. Second-order Møller−Plesset (MP2) calculations were used to determine the optimal interaction geometry of H₂ with aromatic molecules and to examine the effects of pendant functional groups on the interaction energy.[19] For H₂ above the centroid of the phenyl ring and oriented perpendicular to it, the interaction energy could be enhanced by ∼15% by functionalization of benzene with an electron-donating group such as methyl or amino. The bromo
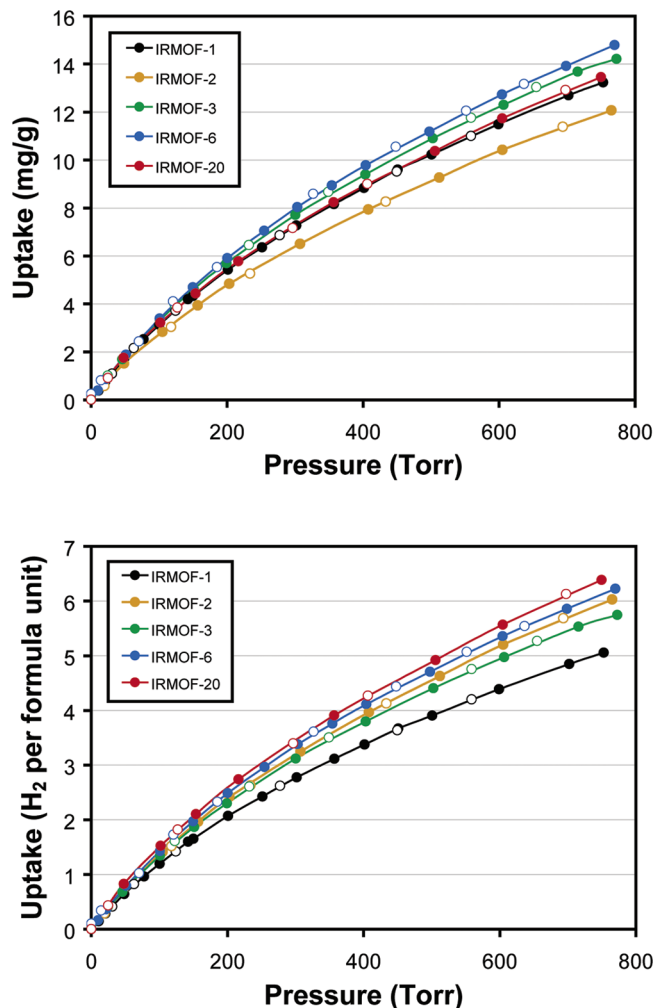
(19) Hübner, O.; Glöss, A.; Fichtner, M.; Klopper, W. *J. Phys. Chem. A* **2004**, *108*, 3019.

Figure 2. Dihydrogen adsorption isotherms for noncatenated IRMOFs measured at 77 K in gravimetric units (top) and normalized per Zn_4OL_3 formula unit (bottom). Data for IRMOF-1 is shown for comparison. Adsorption data are shown as closed circles, desorption data as open circles, and connecting traces are guides for the eye.

substituent (not studied in ref 19) is a weak electron-withdrawing group, but may compensate for the small associated decrease in interaction energy between H₂ and the ring by stronger direct interaction between H₂ and Br due to the greater polarizability of Br. The presence of two coordinated carboxylate groups on the links (found to be slightly activating for the case of −COOLi[19,20]) may overshadow all of these minor differences.

(20) Sagara, T.; Klassen, J.; Ganz, E. *J. Chem. Phys.* **2004**, *121*, 12543.

Thus, the isolated interaction of H_2 with the organic links in the IRMOFs studied here should not differ appreciably.

More importantly, another MP2 computational study has suggested that binding on the inorganic $Zn_4O(O_2C-)_6$ units is considerably stronger than on the links,[20] and this was demonstrated experimentally by single-crystal X-ray and neutron diffraction studies of gases (Ar, N_2, and H_2) adsorbed on IRMOF-1.[21,22] With decreasing temperature, the localization of adsorbate molecules at discrete sites on the framework was evidenced by regions of increased electron (or nuclear) density. The site of highest occupation, and therefore greatest interaction energy, was located on one set of faces of the metal oxide unit, equidistant to three carboxylates. Since there are four of these principle binding sites (denoted $\alpha(\mathbf{CO_2})_\mathbf{3}$) per formula unit, we see from the isotherm data that adsorption at these sites could account for the majority of the uptake in these materials at 77 K and 1 atm, although it is expected that at this temperature adsorbed H_2 diffuses between sites on the framework, as modeled for zeolite Na-A.[23] Inelastic neutron scattering studies of H_2 in IRMOFs indicates this is indeed the case. [5,24]

Although the interaction energy of dihydrogen with the organic links of these materials is believed to be similar in magnitude, the functionalized IRMOFs do demonstrate larger uptake under these conditions than IRMOF-1, by up to 25% on a molar basis (Figure 2). For IRMOF-2, -3, and -6, this may be explained by the constriction of the small pores (where the phenylene edges point inward) by the pendant groups. The pore diameters of the ordered $Pa\bar{3}$ structures are reduced to 9.6−9.8 Å from 12.1 Å in IRMOF-1, whereas the diameters of the large pores (15.0 Å) are unaffected since the phenylene faces point inward, except for IRMOF-2 (12.8 Å) where the steric demand of the bromo group twists the phenylene ring out of the plane of the carboxylate groups. Reduction in pore size is well-known to enhance the interaction energy when the attractive potential fields of opposite walls overlap.[25] It is possible that simply decreasing the interaction distances in the small pore by adorning the links with pendant groups, regardless of their chemical nature, is sufficient to slightly raise the average interaction potential and improve the uptake beyond that primarily associated with the sites on the inorganic clusters. On a gravimetric basis, however, it is clear that the increased uptake by this strategy is moderated by the increased framework mass, and heavier pendant groups (such as bromo) instead result in decreased gravimetric capacity (see Figure 2). Therefore, this does not appear to be a promising strategy for improving the hydrogen uptake by these materials.

IRMOF-20, composed of links that are both longer and narrower than the phenylene-based links, has the largest pores, yet displays the largest uptake on a molar basis. It is concluded that the polarizability of the thieno[3,2-*b*]thiophene group is indeed sufficiently enhanced to improve the uptake despite the increased distance between the links. Here too, however, the inclusion of heavier S atoms reduces any gain in gravimetric capacity.

Catenated IRMOFs. An alternative strategy for reducing the pore dimensions of IRMOFs is catenation. The interpenetration of two or more frameworks has traditionally been considered an obstacle to producing highly porous frameworks due to the resultant reduction of pore volume. Interweaving, the catenation of two or more frameworks with minimal displacement, has in contrast been cited as beneficial where structural reinforcement may prevent framework collapse.[26] The incidence of catenation is favored by the use of longer links, and for framework topologies that are self-duals. These topologies are typically highly symmetric and commonly occurring,[27] such as that which underlies the IRMOF series. In our initial studies of H_2 adsorption in this series of materials, we observed that catenated IRMOF-11 yielded the largest uptake.[6] More recently, high-pressure dihydrogen adsorption was demonstrated in four-fold catenated IRMOFs linked by bis(4-carboxyphenyl)binaphthyl derivatives, despite their smaller pore volumes.[28] In this report, we have examined two more catenated structures.

IRMOF-9 and -13 were synthesized by a method similar to that for the other IRMOFs. Due to the smaller solubilities of the larger links, *N,N*-dimethylformamide was used as the solvent. Activation was performed using chloroform. Following room temperature activation, dinitrogen adsorption measurements confirmed the porosity of the samples, which displayed surface areas and pore volumes comparable to those of IRMOF-11 (see Table 1). A comparison of the measured values to those calculated from the crystal structure data revealed trends similar to those observed for the noncatenated IRMOFs discussed above. Calculated surface areas and pore volumes for the noncatenated analogues were substantially larger, supporting the correct identification of these phases.

Just as for IRMOF-11, the powder X-ray diffraction pattern of the evacuated sample of IRMOF-13 confirmed its identity as that of the catenated phase, whereas IRMOF-9 loses crystallinity (see Supporting Information). Despite exploration of other activation methods, the crystallinity of IRMOF-9 could not be maintained upon evacuation; yet in all cases the resulting samples were highly porous. A comparison of the crystal structures[16] of IRMOF-9 and -11 (or -13) reveals that the mode of catenation is not the same. The two frameworks of IRMOF-11 (or -13) are interwoven such that there is minimal separation between the inorganic SBUs, resulting in facial interactions of the clusters, as well as edge−edge interactions of the links in the $\{2\bar{1}0\}$ planes. In contrast, there is a greater distance between the clusters in IRMOF-9, presumably to the advantage of C−H⋯π interactions between the links. Desolvation of the as-synthesized form disrupts these weaker interactions, and the two frameworks become misaligned. The retention of permanent porosity indicates that the frameworks are, for the most part, still intact. Due to the loss of crystallinity of this material, discussion of relationships between its H_2 adsorption properties and the crystal structure of the as-synthesized form will be

(21) Rowsell, J. L. C.; Spencer, E. C.; Eckert, J.; Howard, J. A. K.; Yaghi, O. M. *Science* **2005**, *309*, 1350.

(22) Spencer, E. C.; Howard, J. A. K.; McIntyre, G. J.; Rowsell, J. L. C.; Yaghi, O. M. *Chem. Commun.* **2006**, 278.

(23) Anderson, C.-R.; Coker, D. F.; Eckert, J.; Bug, A. L. R. *J. Chem. Phys.* **1999**, *111*, 7599.

(24) Rowsell, J. L. C.; Eckert, J.; Yaghi, O. M. *J. Am. Chem. Soc.* **2005**, *127*, 14904.

(25) Everett, D. H.; Powl, J. C. *J. Chem. Soc., Faraday Trans. 1* **1976**, *72*, 619.

(26) Chen, B.; Eddaoudi, M.; Hyde, S. T.; O'Keeffe, M.; Yaghi, O. M. *Science* **2001**, *291*, 1021.

(27) Ockwig, N. W.; Delgado-Friedrichs, O.; O'Keeffe, M.; Yaghi, O. M. *Acc. Chem. Res.* **2005**, *38*, 176.

(28) Kesanli, B.; Cui, Y.; Smith, M. R.; Bittner, E. W.; Bockrath, B. C.; Lin, W. *Angew. Chem., Int. Ed.* **2005**, *44*, 72.
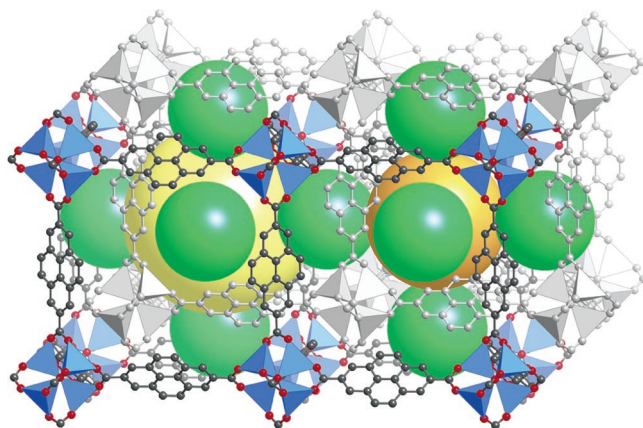
Figure 3. Schematic representation of the pore structure in IRMOF-13. The catenation of two frameworks, one shown in grayscale, reduces the fixed diameters of the large and small pores defined by either framework alone (yellow and orange spheres, compare IRMOF-20 in Figure 1). Additional smaller voids are formed, shown as green spheres, which account for roughly 45% of the pore volume. Atom colors: C black, O red, Zn blue tetrahedra, H not shown.

limited, but it should be noted that its crystal density was used to estimate the pore volume in units of cm^3/cm^3 in Table 1, and the pore dimensions from the crystal structure are comparable to those of IRMOF-13 despite the differences in their framework orientations.

The interweaving of IRMOF frameworks results in a larger effective thickness of the walls and concomitant reduction of the pore diameters. The specific consequences on the pore structure are discussed below for IRMOF-13 and illustrated in Figure 3. Similar to those of the noncatenated IRMOFs, the pore structure can be viewed as three approximately orthogonal sets of channels which intersect at large cavities. In noncatenated cubic IRMOFs these channels lie along the principle cell axes, while in IRMOF-13 they are directed along [241], [42$\bar{1}$], and [2$\bar{2}$1]. The catenation of two frameworks significantly reduces the fixed diameters of the pores (12.4 and 8.7 Å, respectively), and as a result, these pores no longer intersect. Instead, the depth of the apertures connecting them increases and may be considered as small secondary voids 7 Å in diameter. There are one large pore, one small pore, and six apertures defined by four Zn_4OL_3 formula units; therefore, the fraction of the total volume associated with the apertures is substantial, ~45%. Further, the apertures are bounded by the edges of two inorganic clusters, where it is believed the interaction energy is higher. The total reduction of the free and fixed diameters in the pore structure should then enhance the heat of adsorption due to the increased overlap of the attractive potential of opposite walls.[25]

The advantage of constricting the pore dimensions in catenated IRMOFs is demonstrated by their higher adsorption of H_2 at low pressure. As shown in Figure 4, IRMOF-13 outperforms IRMOF-1 across the entire range of pressure examined. When these results are scaled for the increased mass of the pyrene link, the uptake at 1 atm is nearly double that of IRMOF-1, despite this material's substantially larger pore volume. Notably, the uptake at low pressure is considerably larger, i.e. the Henry's law constant (isotherm slope as $P{\rightarrow}0$) is greater, indicating the heat of adsorption has indeed been enhanced. This was investigated by isosteric analysis, and is discussed in greater detail below. The measured uptake for
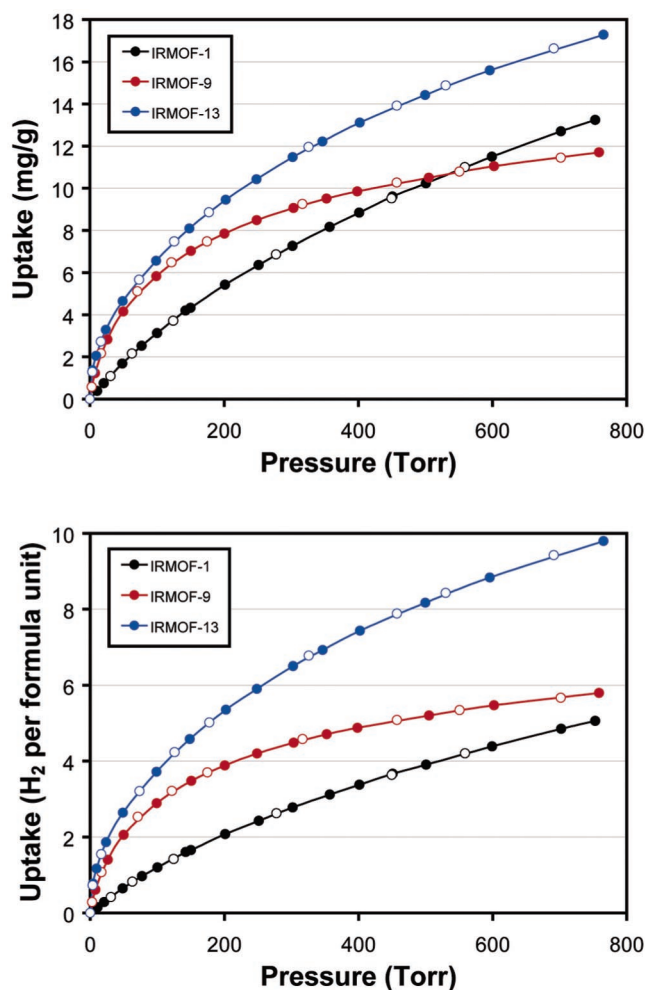

Figure 4. Comparison of dihydrogen adsorption isotherms for catenated IRMOFs and IRMOF-1 measured at 77 K in gravimetric units (top) and normalized per Zn_4OL_3 formula unit (bottom). Adsorption data are shown as closed circles, desorption as open circles, and connecting traces are guides for the eye.

IRMOF-13 is ~10% greater than that previously reported for IRMOF-11[6] and seems to indicate the fully aromatic pyrene link gives rise to a slightly higher interaction energy.

IRMOF-9 shows similar uptake at low pressure, but the rate of increase in uptake with pressure (isotherm slope) drops considerably above 100 Torr (see Figure 4). Due to the loss of crystallinity of the sample, it is difficult to interpret these results on the basis of structural aspects. It is clear from the large pore volume measured for this material (Table 1) that it is comparable to those of the other samples. If the reorientation of the frameworks upon desolvation results in local interweaving (perhaps of fragments of the frameworks) in a manner similar to that of IRMOF-13, then the corresponding pore dimensions would be slightly larger due to the smaller width of the biphenyl link. It is also possible that there is local flexibility in link conformation and/or relative orientation of the two frameworks, and therefore the difference in the shape of the H_2 isotherm is related to an activated process; however, no hysteresis was observed.

MOFs Composed of $Cu_2(O_2C-)_4$ and $[Zn(O-)(O_2C-)]_\infty$ SBUs. The dihydrogen adsorption capacities of isoreticular MOFs, based on cubic reticulations of the $Zn_4O(O_2C-)_6$ secondary building unit, have been demonstrated to be influ-

enced primarily by the metrics of the links. We have shown that the H$_2$ uptake is enhanced by reducing the pore dimensions in this chemically related series of materials. To further improve both the capacity and heat of adsorption in MOFs, it is necessary to present adsorptive sites with greater interaction potentials while maintaining a large total pore volume with appropriate pore dimensions. Thus, frameworks composed of other inorganic clusters should be explored. We have identified the square Cu$_2$-(O$_2$C−)$_4$ "paddlewheel" as a promising SBU in this regard. Many MOFs displaying a variety of network topologies have been identified using this building unit, or analogues composed of other transition metals.[7,26,29,30] The use of copper(II) is the most attractive, as its propensity toward Jahn−Teller distortion weakens the bonding of nucleophiles, such as solvent molecules, at the axial sites. Removal of these species exposes open metal sites and Cu$^{\delta+}$−O$^{\delta-}$ dipoles on the surface that are expected to increase the local interaction energy for adsorptives. Experimental support for this hypothesis was recently reported for a new framework based on the NbO-net, which reversibly adsorbs 2.47 wt % H$_2$ at 77 K and 1 atm.[30]

In this study, we examine the adsorption properties of the material HKUST-1, a MOF composed of copper(II) paddlewheel clusters linked by trigonal benzene-1,3,5-tricarboxylate.[31] The structure is cubic, based on the augmented twisted boracite net.[32] The pore structure is similar to the IRMOFs in that it can be viewed as three mutually perpendicular arrays of channels that intersect at cavities that are 13.2 and 11.1 Å in diameter, with apertures 6.9 Å in diameter. The faces of 12 paddlewheel SBUs (i.e., the open metal sites) point inward to the large pores, whereas the edges of 12 SBUs line the smaller pores. In addition, there are small secondary pores that are only 6.9 Å in diameter, accessible through 4.1 Å windows, which are bounded by six SBU edges. The calculated pore volume of this material is between 62 and 72% (see Table 1), and thus we recognize it fulfills the criteria of large pore volume with small dimensions.

The synthesis of this material has been revisited previously for examination of its applicability in gas separation[33] and catalysis.[34] Both groups noted the importance of mild solvothermal conditions for preparing samples free of Cu$_2$O impurities. We observed that high-purity samples of well-formed crystallites could be prepared at low temperatures within days from the mixed solvent DMF/H$_2$O/ethanol. The most porous samples were also produced when a solvent activation step was employed. Although immersion in chloroform and evacuation at elevated temperatures yields samples with large measured pore volumes, it was determined that

immersion in dichloromethane followed by overnight heating to 170 °C under vacuum gave the best results. This is in contrast to a previous report of framework decomposition in dichloromethane at room temperature; however, our observation of the reversible color change (turquoise to deep violet) upon dehydration and the agreement of experimental and calculated PXRD patterns are consistent with those described in that work.[34] The dinitrogen isotherm measurements revealed our improved evacuation procedure produces samples with even larger apparent surface areas and pore volume (see Table 1).

Another material that was explored for the presence of high-energy adsorptive sites upon evacuation is MOF-74. The structure of this material was described recently within the presentation of several new MOFs composed of infinite SBUs, where metal ions are bridged by carboxylates or other functionalities to form rods that can adopt one of 14 invariant packings.[35] MOF-74 is composed of Zn^{2+} ions bridged by the carboxylate and oxy- groups of fully deprotonated 2,5-dihydroxybenzene-1,4-dicarboxylic acid, giving rise to linked chains that are arranged in a parallel, hexagonal manner. The framework defines hexagonal channels that are filled by free solvent molecules, and one molecule of DMF coordinated to a sixth site on each of the octahedral Zn^{2+} centers. In contrast to Cu^{2+}, Zn^{2+} does not exhibit a Jahn−Teller distortion, and oxygen donor ligands are typically bound strongly, hampering their removal under heating conditions that are mild enough to avoid framework collapse. The coordinative flexibility of Zn^{2+} is well-known, however, and it may adopt several coordination geometries with oxygen donor ligands. Successful removal of the bound ligands would open up channels 10.8 Å in diameter, bounded on all sides by exposed Zn$^{\delta+}$−O$^{\delta-}$ dipoles.

It was previously shown that initial activation of as-synthesized MOF-74 with water could exchange the bound DMF molecules within the channels. Subsequent heating at >200 °C was required for the removal of water, yielding a material with a Langmuir surface area of 245 m^2/g.[35] Porosity calculations (see Table 1) indicated this value could be improved substantially. After optimizing the synthesis to yield gram-scale quantities, a number of activation procedures were explored. It was discovered that immersion of the material in methanol, followed by considerable heating under vacuum yielded samples with substantially larger apparent surface areas. The removal of the majority of DMF was confirmed by elemental analysis and FT-IR. Although several of the characteristic bands of DMF overlap those of the MOF, the bands at 2929, 1654, 1498, 1109, and 1060 cm^{-1} could be discerned, and these are absent in the methanol-exchanged and evacuated samples. Interestingly, both elemental analysis and FT-IR revealed that only a small fraction of the DMF (∼15%) was exchanged by ethanol, despite extended immersion in the solvent. It is spatially possible for ethanol to diffuse into the water-filled channels of the as-synthesized material; however, its larger size and/or lower polarity significantly hinders the exchange process.

Powder X-ray diffraction confirmed that the evacuated material maintained crystallinity, despite a noticeable reduction

(29) (a) Chen, B.; Eddaoudi, M.; Reineke, T. M.; Kampf, J. W.; O'Keeffe, M.; Yaghi, O. M. *J. Am. Chem. Soc.* **2000**, *122*, 11559. (b) Bourne, S. A.; Lu, J.; Mondal, A.; Moulton, B.; Zaworotko, M. J. *Angew. Chem., Int. Ed.* **2001**, *40*, 2111. (c) Eddaoudi, M.; Kim, J.; Vodak, D.; Sudik, A.; Wachter, J.; O'Keeffe, M.; Yaghi, O. M. *Proc. Natl. Acad. Sci. U.S.A.* **2002**, *99*, 4900. (d) Eddaoudi, M.; Kim, J.; O'Keeffe, M.; Yaghi, O. M. *J. Am. Chem. Soc.* **2002**, *124*, 376. (e) Abourahma, H.; Bodwell, G. J.; Lu, J.; Moulton, B.; Pottie, I. R.; Walsh, R. B.; Zaworotko, M. J. *Cryst. Growth Des.* **2003**, *3*, 513.
(30) Chen, B.; Ockwig, N. W.; Millward, A. R.; Contreras, D. S.; Yaghi, O. M. *Angew. Chem., Int. Ed.* **2005**, *44*, 4745.
(31) Chui, S. S.-Y.; Lo, S. M.-F.; Charmant, J. P. H.; Orpen, A. G.; Williams, I. D. *Science* **1999**, *283*, 1148.
(32) O'Keeffe, M.; Eddaoudi, M.; Li, H.; Reineke, T.; Yaghi, O. M. *J. Solid State Chem.* **2000**, *152*, 3.
(33) Wang, Q. M.; Shen, D.; Bülow, M.; Lau, M. L.; Deng, S.; Fitch, F. R.; Lemcoff, N. O.; Semanscin, J. *Microporous Mesoporous Mater.* **2002**, *55*, 217.
(34) Schlichte, K.; Kratzke, T.; Kaskel, S. *Microporous Mesoporous Mater.* **2004**, *73*, 81.

(35) Rosi, N. L.; Kim, J.; Eddaoudi, M.; Chen, B.; O'Keeffe, M.; Yaghi, O. M. *J. Am. Chem. Soc.* **2005**, *127*, 1504.
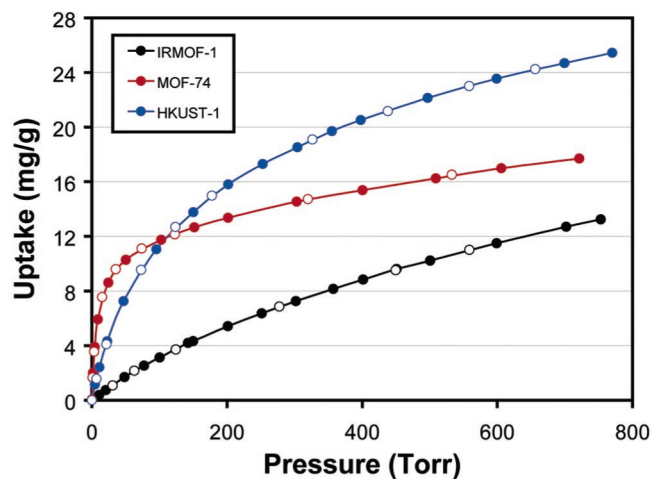
Figure 5. Comparison of the dihydrogen adsorption isotherms of HKUST-1, MOF-74, and IRMOF-1 measured at 77 K. Adsorption data are shown as closed circles, desorption as open circles, and connecting traces are guides for the eye.

in particle size (visually observed). The reflections from samples heated to 320 °C were slightly broadened from those heated to 270 °C, and the samples were comparable in porosity. Shifts in observed reflections with $l \neq 0$ were recorded, indicating a compression of the c axis upon evacuation (see Supporting Information). The pattern was indexed to a rhombohedral cell with $a = 26.14(2)$ Å, $c = 6.300(5)$ Å. The compression of the cell is a result of relaxation of the bonding environment about the five-coordinate Zn^{2+} upon loss of the coordinated methanol. Simulation of the pattern using the compressed cell with all solvent atoms removed matched the observed intensities. In addition to the FT-IR and elemental analysis data, we conclude that the pores of this material were essentially evacuated of their contents.

With these two materials in hand, we examined the effects of their unique pore environments by comparing their H_2 adsorption isotherms. As shown in Figure 5, both materials offer a significant improvement over those discussed above. The isotherm of IRMOF-1 is plotted for comparison. Both HKUST-1 and MOF-74 demonstrate much stronger binding of H_2 in the low-pressure region, and they outperform the IRMOF materials on a gravimetric basis across the entire pressure range examined. The amount adsorbed per gram by HKUST-1 is approximately double that of IRMOF-1 at 1 atm (see Table 1) and is marginally larger than that of MOF-505,[30] which is also composed of open Cu^{2+} sites. It is apparent that this structural element is beneficial for the improvement of H_2 adsorption under these conditions.

The isotherm measured for MOF-74 has a particularly large initial slope, which begins to decrease sharply at 50 Torr. The amount adsorbed at this pressure is 10 mg/g, equivalent to 0.8 H_2 per Zn. This feature indicates that dihydrogen is strongly adsorbed near the open metal sites lining the pore, but as these sites become filled (expected to occur at ~1 H_2 per Zn), the increase in uptake with pressure declines as dihydrogen interacts with weaker secondary sites. This observation provides additional evidence that gains in the low-pressure uptake of H_2 in MOFs can be achieved by stabilizing coordinatively unsaturated centers on their surfaces.

Isosteric Analysis of the Heat of Adsorption. Analysis of the temperature dependence of dihydrogen adsorption by MOFs

provides further insights into the influences their structural features exert. Isosteric analysis of adsorption isotherms collected at various temperatures allows an estimation of the coverage-dependent isosteric heat of adsorption (Q_{st}), where the behavior of this function is determined by the relative magnitudes of the adsorbent−adsorbate and adsorbate−adsorbate interactions.

Dihydrogen adsorption isotherms were collected using a volumetric technique at 77, 87, and 195 K for IRMOF-1, IRMOF-11, HKUST-1, and MOF-74. The samples were synthesized, activated, and outgassed according to the optimal procedures described above and yielded surface areas and pore volumes (measured by N_2 adsorption at 77 K) comparable to those determined by the gravimetric method. The data are shown in Figure 6; for consistency, the data were converted to gravimetric units by the factor 9.0 mg H_2 per 100 cm^3 at STP. As expected, the amount adsorbed decreases significantly with temperature, and at 195 K the uptake is <0.5 mg/g at 1 atm for all samples. The 77 K data is consistent with the gravimetric results in terms of magnitude of uptake, isotherm curvature, and absence of hysteresis. In general, the converted values are ~10% greater than those determined gravimetrically, which could stem from the different dead-volume and buoyancy corrections used in these two complementary methods. While individual samples gave repeatable isotherms on each instrument that were essentially coincident, and these were further reproducible for different samples synthesized and activated in the same manner, this comparison of techniques provides a reasonable estimate of the actual uncertainty in the measurements, each ±5%. This is an acceptable variance for adsorption measurements, which have long been known to be instrument and sample dependent.

Attempts to fit the isotherms to many of the commonly used empirical equations did not yield satisfactory results. The unique curvatures of the MOF-74 isotherms, in particular, were poorly described by even the four-parameter Generalized Langmuir and Dubinin−Astakhov equations.[36] To extract the coverage-dependent isosteric heat of adsorption, the data were modeled with a virial-type expression composed of parameters a_i and b_i that are independent of temperature:[37]

$$\ln P = \ln N + \frac{1}{T}\sum_{i=0}^{m}a_i N^i + \sum_{i=0}^{n}b_i N^i \qquad (1)$$

where P is pressure, N is the amount adsorbed (or uptake), T is temperature, and m and n determine the number of terms required to adequately describe the isotherm. Aspects of this equation and its use in studying CH_4, CF_4, SF_6, and H_2 adsorbed on activated carbons have been described previously.[38] For each material, global fittings of the data with and without inclusion of the 195 K values were performed using unity weights. Successive terms were included in the fitting expression until they did not appreciably reduce the χ^2 goodness-of-fit; in all

(36) Further discussion of the development and interpretation of isotherm models can be found in Rudzinski, W.; Everett, D. H. *Adsorption of Gases on Heterogeneous Surfaces;* Academic Press: London, 1992 and Jaroniek, M.; Madey, R. *Physical Adsorption on Heterogeneous Solids*; Elsevier: Amsterdam, 1988.
(37) Czepirski, L.; Jagiello, J. *Chem. Eng. Sci.* **1989**, *44*, 797.
(38) (a) Jagiello, J.; Bandosz, T. J.; Putyera, K.; Schwarz, J. A. *J. Chem. Eng. Data* **1995**, *40*, 1288. (b) Ansón, A.; Jagiello, J.; Parra, J. B.; Sanjuán, M. L.; Benito, A. M.; Maser, W. K.; Martínez, M. T. *J. Phys. Chem. B* **2004**, *108*, 15820.
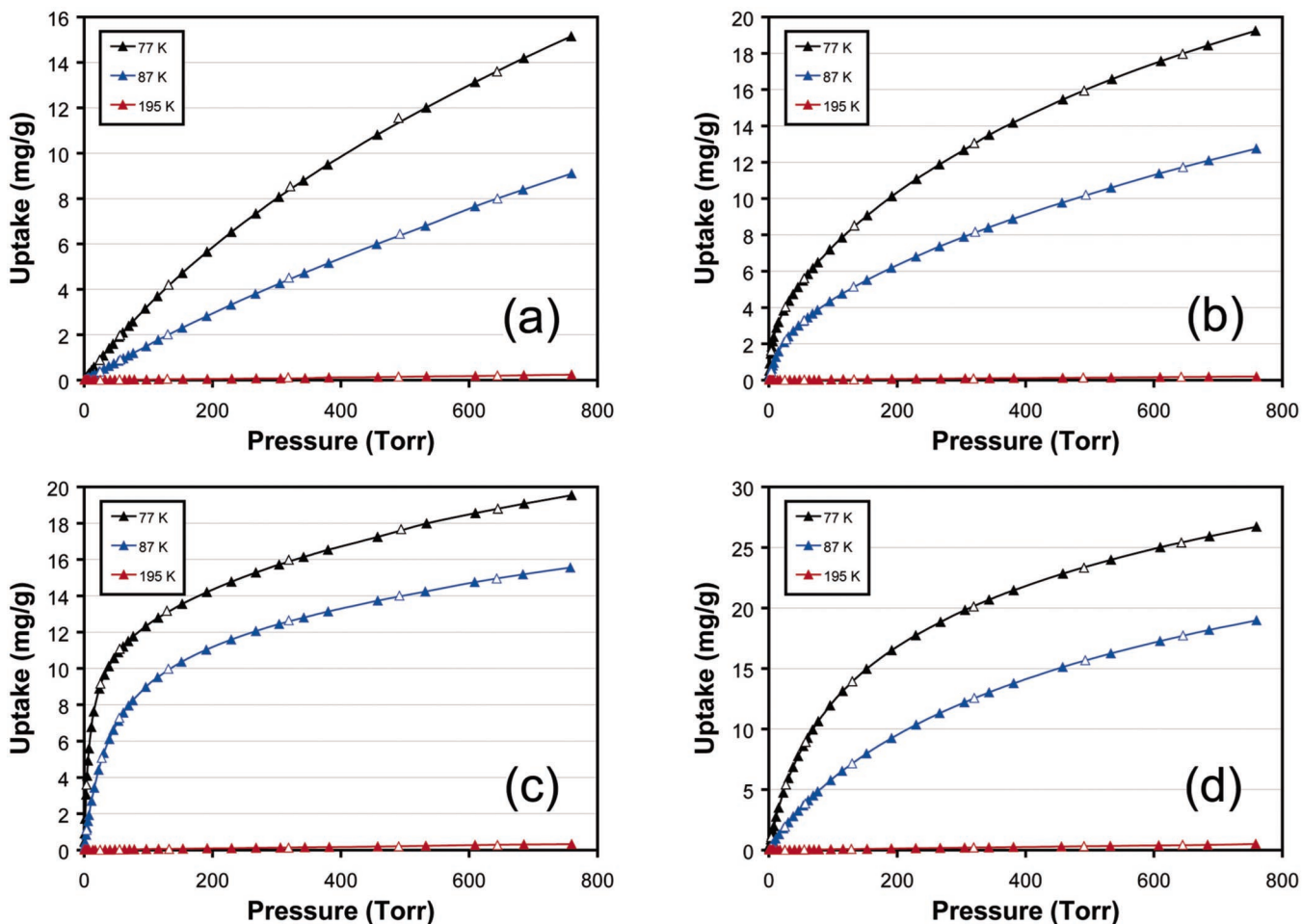
Figure 6. Dihydrogen adsorption isotherms measured at various temperatures for (a) IRMOF-1, (b) IRMOF-11, (c) MOF-74, and (d) HKUST-1. Note the different scales on ordinate axes. Adsorption data are shown as closed triangles, desorption as open triangles, and connecting traces are guides for the eye.

cases $m \leq 6$ and $n \leq 3$ (see Supporting Information). From these results, the isosteric heat of adsorption is calculated according to:

$$Q_{st} = -R \sum_{i=0}^{m} a_i N^i \qquad (2)$$

where R is the universal gas constant. The coverage dependencies of Q_{st} calculated from fitting the 77 and 87 K data are presented graphically in Figure 7. Errors were propagated by taking into account the covariance of the fitting parameters. An inherent instrumental error of 2% in pressure was estimated by fitting replicate measurements made on HKUST-1, which is comparable to instrumental specifications. Thus, the calculated errors are underestimated as they do not reflect sample variance. Due to the small uptake (amount adsorbed) at 195 K by each material, inclusion of these data in the fitting can provide estimates of the Q_{st} only at very low coverage. For HKUST-1 and MOF-74, these values agreed with the 77 and 87 K data fits within 5% but deviated by ~10% for IRMOF-1 and -11.

As expected, the behavior of the isosteric heat of adsorption is unique to each MOF. The larger-pore materials, IRMOF-1 and HKUST-1, show gradual, nearly linear decrease in their values as functions of the amounts adsorbed. The isosteric heat at low coverage is 2.0 kJ/mol larger for HKUST-1, providing further evidence that H₂ interacts more strongly with the Cu₂-
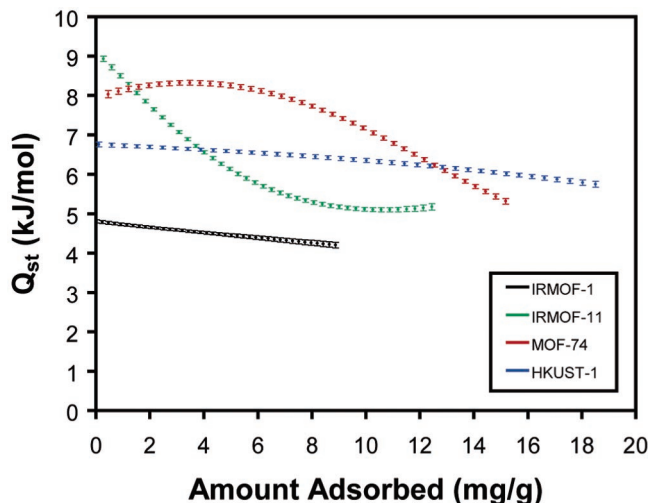

Figure 7. Coverage dependencies of the isosteric heats of adsorption for H₂ in MOFs calculated from fits of their 77 and 87 K isotherms. Error bars represent one standard deviation.

$(O_2C-)_4$ cluster than $Zn_4O(O_2C-)_6$. No evidence is found for strong binding in the small 6.9 Å secondary pores of HKUST-1 under these conditions. In contrast, the heat of adsorption at low coverage is 9.1 kJ/mol for IRMOF-11 and drops off considerably with the amount adsorbed to about 5.1 kJ/mol at the limits of the interpolation. This is an indication of the presence of strong binding sites within the material, which

become saturated at ~10 mg/g (5.7 H_2 per Zn_4OL_3 formula unit). Given the low Q_{st} values observed for IRMOF-1, it is concluded that the stronger interactions in IRMOF-11 must be due to the constrictions in the framework that allow overlap of the attractive potential of proximal surfaces. After these regions are occupied (assuming a static model, which is certainly a simplification at this temperature), H_2 is then adsorbed in the larger pores in IRMOF-11, which are still considerably smaller than IRMOF-1 and therefore lead to the observed larger heats of adsorption. Finally, MOF-74 displays the largest isosteric heat of adsorption over much of the range of coverage measured. Interestingly, these values increase with coverage until a maximum of 8.3 kJ/mol at 3.5 mg/g (0.28 H_2 per Zn), inferring that adsorbate−adsorbate interactions are nonnegligible at low coverage. Clearly, the small pore dimensions and unsaturated metal sites aid in the low-pressure uptake by this material.

These values of the heat of adsorption can be compared with those in the literature for other microporous materials. An early study compared the adsorption of H_2 and D_2 on charcoal in the temperature range 17−90 K, from which the isosteric heat of adsorption was shown to smoothly decrease from 7.3 to 1.4 kJ/mol at high loading (values read from their plot).[39] The values for D_2 were ~0.75 kJ/mol larger. In the context of H_2 isotopic separations, six adsorbents were analyzed in the temperature and pressure ranges of 75−90 K and 0−1 atm, respectively.[40] The isosteric heats were found to range between 7.9 and 6.0 kJ/mol (with increasing coverage) for two different charcoals; 7.3 and 5.4 kJ/mol for silica gel; and 7.9 and 5.9 kJ/mol for three different zeolites (types 4A, 5A, and 13X; probably incompletely dehydrated). Using an analysis similar to that described here, the Q_{st} at low coverage was found in the 7−7.5 kJ/mol range for microporous carbons after various chemical activations.[38b] These values decreased monotonically with coverage to ~5 kJ/mol over the range examined. Using a large number of data collected between 77 and 273 K for pressures up to 6 MPa, Q_{st} was determined to be between 6.3 and 5 kJ/mol for the high surface area carbon AX-21.[2a] A recent study found values between 5.2 and 3.9 kJ/mol for a variety of functionalized activated carbons by analysis of data in the temperature range 77−114 K.[41] Larger values of Q_{st} appear to be achievable with zeolites; 10.7−6.2 kJ/mol was calculated for zeolite Na-A using data collected between 40 and 120 K.[42]

Estimates of the heat of adsorption for dihydrogen in MOFs have also appeared recently. IRMOF-1 was investigated independently and found to have values ~0.5 kJ/mol greater than our measurements.[9] In comparison, the small pores of Prussian blue analogues[9] and a magnesium-containing MOF[43] were found to enhance the heat of adsorption considerably, up to 9.5 kJ/mol at low coverage, consistent with expectation. Independent results for dihydrogen adsorption by HKUST-1 estimate Q_{st} as 6.6−5.8 kJ/mol in the uptake range of 0−8 mg/g;[44] this is comparable to the findings presented here but shows a greater rate of decrease with coverage. The material prepared in that study was synthesized and evacuated under different conditions

(no solvent activation, evacuation at 100 °C for 6−8 h), which lead to a considerably less porous material with smaller H_2 uptake (14.4 mg/g at 1 atm, 77 K).

Concluding Remarks

Low-pressure, low-temperature dihydrogen adsorption data have been presented for six porous Zn_4O-based MOFs, many of which have been prepared in gram quantities for the first time. In conjunction with dinitrogen adsorption studies and structural calculations, the effects of link functionalization and catenation on the H_2 adsorption properties of these materials have been examined. While functionalization of the link does not have a pronounced influence on the amount adsorbed by this series of compounds, catenation and the concurrent reduction in pore dimensions leads to a significant enhancement under the conditions examined. The catenated materials display larger Henry's Law constants in the limit of low coverage, as well as typically larger fractions of pore volume filled by H_2, denoted f_{H2} and summarized in Table 1. This value is defined in the caption of Table 1 as the equivalent volume of H_2 in its liquid state adsorbed (at 1 atm, 77 K) as a fraction of the pore volume of the material, determined by N_2 adsorption, and is therefore structure independent. Over 30% of the pore volume of IRMOF-13 is filled by H_2; in contrast, IRMOF-20 has the largest capacity for N_2, but the pores are the least filled by H_2 under these conditions. In principle, the value of f_{H2} can be used to estimate the saturation capacity of each material, assuming liquid H_2 filling of the pores. While this predicts very attractive capacities, i.e., 10.8 wt % for IRMOF-20, the actual density of H_2 at saturation is not known, and it is more prudent to determine these values experimentally.

The data presented here suggest that, with the exception of imparting catenation, the role of the links in dihydrogen adsorption is rather minor under these conditions. Recent computational and experimental work has pointed to the inorganic clusters as providing the most attractive binding sites, and enhanced physisorption of dihydrogen by MOFs containing coordinatively unsaturated metal sites was demonstrated. The structure−property correlations have been corroborated by calculated coverage-dependent isosteric heats of adsorption. By comparison with data collected for catenated and noncatenated IRMOFs, it has been shown that alteration of the inorganic adsorption sites has a significant impact on the dihydrogen interaction under these conditions. Appropriate pore dimensions are still recognized as a major contributor to the heat of adsorption at low loading; however, a large pore volume is essential for improving the total H_2 uptake. This is illustrated by the relative slopes of the 77 K dihydrogen isotherms measured for HKUST-1 and MOF-74 (Figure 5) and the estimated fractions of their pore volumes filled by liquid H_2, f_{H2} (see Table 1). Although the pores are larger in HKUST-1 and its isosteric heat of adsorption is smaller than that of MOF-74 at low loading, the larger pore volume of HKUST-1 leads to greater capacity and suggests a larger gain in capacity before saturation is achieved.

Finally, the H_2 capacities measured for these materials should be compared to reliable values reported for zeolites (up to 7.2 mg/g) and activated carbons (up to 21.4 mg/g) under the same conditions.[2b] This study has focused on the most promising MOFs among the many thousands that have been structurally

(39) van Dingenen, W.; van Itterbeek, A. *Physica* **1939**, *6*, 49.
(40) Basmadjian, D. *Can. J. Chem.* **1960**, *38*, 141.
(41) Zhao, X. B.; Xiao, B.; Fletcher, A. J.; Thomas, K. M. *J. Phys. Chem. B* **2005**, *109*, 8880.
(42) Stéphanie-Victoire, F.; Goulay, A.-M.; Cohen de Lara, E. *Langmuir* **1998**, *14*, 7255.
(43) Dinca, M.; Long, J. R. *J. Am. Chem. Soc.* **2005**, *127*, 9376.
(44) Lee, J. Y.; Li, J.; Jagiello, J. *J. Solid State Chem.* **2005**, *178*, 2527.

characterized. It is conceivable that many thousand more will be identified soon, and it is hoped that this examination has elucidated some useful criteria for the evaluation of new candidate materials for hydrogen storage. Much of the periodic table has yet to be explored in the pursuit of open framework MOFs; it is probable that the inclusion of new inorganic clusters in the assembly process will yield frameworks with even greater affinity for H_2, but this must be coupled with large capacity to pursue practical storage targets.

Supporting Information Available: Crystallographic information file (CIF) of IRMOF-20, PXRD patterns, fitted isotherm data and complete ref 2c. This material is available free of charge via the Internet at http://pubs.acs.org.

JA056639Q